ChemComm

Accepted Manuscript

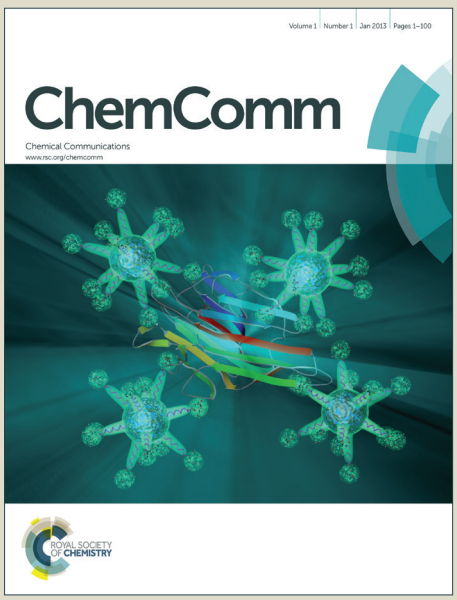

ROYAL SOCIETY OF CHEMISTRY

www.rsc.org/chemcomm

Journal Name

RSCPublishing

COMMUNICATION

Highly-dispersed Boron-doped Graphene Nanoribbons with Enhancing Conductibilities and Photocatalysis

Cite this: DOI: 10.1039/xoxxoooooox

Mingyang Xing, Wenzhang Fang, Xiaolong Yang, Baozhu Tian, and Jinlong Zhang†

Received ooth January 2012,
Accepted ooth January 2012

DOI: 10.1039/xoxxoooooox

www.rsc.org/

Highly-dispersed boron-doped graphene nanoribbons (B-GNRs) were prepared by a simple vacuum activation method, which exhibit p-type semiconductor properties and provide much more Zigzag- and Armchair-edges to facilitate the controlling of bandgap. B-GNRs are used to photodegradation of Rhodamine B to demonstrate their excellent conductivities and photocatalytic activities.

Graphene (GR), as an exciting two-dimensional material with its high crystallinity and interesting semimetal electronic properties, has attracted much more attention since 2004.[1] In order to give the single-layer graphene certain special electrical characteristics, the large scaled graphene was cut into small nanoribbons through some chemical technology.[2] Structures of the graphene nanoribbons (GNRs) with high electrical conductivity, high thermal conductivity, low-noise, which make the GNRs have a large potential in the application of producing integrated circuit. In addition, when the size of GNRs was limited to 10-20 nm width, the electrons are confined in a small area to emerge some semiconductor properties, because of the electronic accumulation making graphene achieve an "off" state.[3] In accordance with the border structures, GNRs are divided into zigzag GNRs (ZZ-GNRs) and armchair GNRs (AC- GNRs). Though both of them have the bandgaps,[4] but ZZ-GNRs are more inclined to the semimetal with excellent conductivity,[5] and AC-GNRs are more like a semiconductor with tunable bandgaps.[6] As an ideal semiconductor, GNRs exposed with both ZZ- and AC-edges are supposed to replace silicon for the preparation of transistor and other photoelectric devices.[2b, 7] Additionally, the excellent conductivity and tunable bandgap also make GNRs have a solar light response, which determines its potential application in photoelectrochemical devices and photocatalysis. Hence, the realization of the controllable and scalable production of GNRs is of great importance for its application in areas ranging from transistors to photocatalysis.

On the other said, study on the electric properties of impurity doping graphene nanoribbons is a research hotspot in recent years. Leon et al.[8] have investigated the electronic properties of the nitrogen doped ZZ-GNRs, and found the strong change of the localized electronic spectrum of N-GNRs. Wang et al.[9] also have successfully prepared a nitrogen doped GNRs by nitrogen species through high-power electrical joule heating in ammonia gas, which is leading to a n-type electronic doping. Actually, under normal conditions, the doping modification on graphene is easy to cause the showing of p-type transfer properties, especially the nitrogen or boron doping. For instance, Tang et al.[10] reported tunable bandgaps and p-type transport properties of B-doped graphenes that were achieved via controllable doping through reaction with the ion atmosphere of trimethylboron decomposed by microwave plasma. Theoretical studies on GNRs doped with B atoms have demonstrated that the edge-type, as well as the substitutional doping, could induce a half-metallic behavior and the band gap could be tuned by doping,[2c, 11] which suggested the potential application of B-GR in photocatalysis.

A template chemical vapor deposition (CVD) technology is a general method for controllably producing GNRs,[12] however, the CVD method involves complex chemical reactions, and many by-products are produced in the CVD process. Therefore, although great efforts have been made, scalable production of GR with well-controlled morphologies is still a great challenge and a major obstacle which hampers practical applications of GR. Here, we developed a simple vacuum activation method to successfully prepare the boron doped GNRs (B-GNRs) by using H_3BO_3 as the template. After vacuum activation, the ultrasonic treatment is used to

improve its dispersion. The B-GNRs exhibit high dispersion and semimetallic properties. The B doping cannot destroy the conjugated structure of GNRs but improve its reduction degree by the exposure of ZZ- and AC-edges, which induces the enhancing performance of electrical conductibility and photocatalytic activity of GNRs.

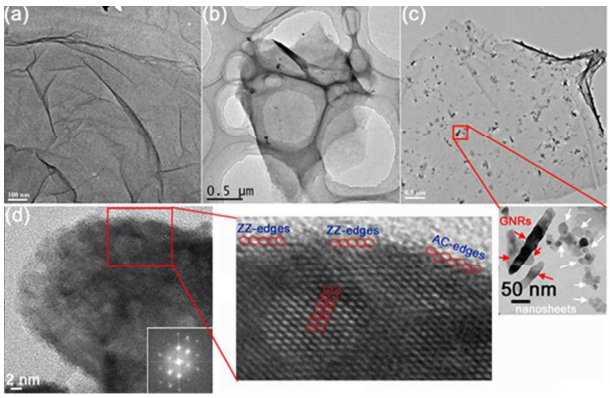

Fig. 1 TEM images for (a) GO, (b) GR, (c) B-GNRs and (d) HRTEM images for B-GNRs. Inset of (d) is the corresponding fast Fourier transform (FFT) pattern.

Fig. 1a is the TEM spectra of the GO, and it has a typical two-dimension structure. After vacuum activation treatment, the brown GO is reduced to the black GR, but its morphology is almost changeless (Fig. 1b), and there are no nanoribbons structure generated in the vacuum reduction process. The Raman spectra also indicate the successful reduction of GO by a simple vacuum activation method (Fig. S1).[13] The band at around 1357 cm^{-1} is common for disordered sp^2 carbon and has been called the D-band. And another band at around 1599 cm^{-1} is close to that observed for well-ordered graphite and is often called the G-band. After vacuum reduction, the G-band shifts from 1599 to 1588 cm^{-1}, which matches the value of pristine graphite, indicating the successfully reduction of GO. Interestingly, when the H_3BO_3 is added in preparation, some GNRs with 150-200 nm length and 20-40 nm width are produced after a vacuum activation treatment, as shown in Fig. 1c. Although there are still some large-scaled graphene existence after boron doping, smaller size structures such as nanoribbons and naonosheets begin to be generated during the vacuum heating and ultrasonic process (inset of Fig. 1c). The nano-sized ribbon structure would give much more edges and facilitate the loading of other nanoparticles, because of the distribution of unreduced carboxylic acid groups on the edges of GRNs. HRTEM characterization in Fig. 1d gives further evidence for the perfect crystalline structure of the GNRs. It is showing a nanoribbon structure, and the layer is nearly monolayer or few-layer graphene, because a hexagonal atomic lattice with uniform contrast can be clearly discerned and the measured distance between carbon atoms of ~0.14 nm agrees well with the theoretical value for graphene.[14] Optical diffraction, also known as fast Fourier transformation (FFT), of Fig. 1d shows a hexagonal pattern, revealing the six-fold symmetry feature of graphene. The perfect lattices indicate the absence of many topical defects in graphene. It is worth noticed that the GRNs have both ZZ-edges and AC-edges in Fig. 1d. Some studies on GR have reported that the edges in GR sheets and few-layer GNRs have highly reactive sites,[15] which could exhibit metallic and semiconductor properties simultaneously.

The XRD results show the absence of the characteristic peak belonging to (002) crystal of GO at 10.14° after the vacuum reduction (Fig. S2), indicating that the GO has been successfully reduced to GR by a vacuum activation process. It is well known that the macro-residual stress induced by the foreign impurity such as boron oxides can cause the anisotropic lattice contraction. When the macro-residual stress is the pressure stress, it will introduce a distinct pressure stress on GR surface to divide the large scaled GR sheet into small pieces of nanoribbons. Much more exposed edges on GR can give a fringe effect and facilitate the further modification on the edge of GR.[2b, 16] In order to prove the role of H_3BO_3 in the generation of GNRs, the TEM spectra of vacuum activated GRs in the absence of H_3BO_3 are shown in Fig. S3a-e. There is no GNRs presence in the absence of H_3BO_3, maybe owing to the absence of pressure stress. With the increase of the ultrasonic time, the size of GR is decrease, but there is still no GNRs presence even though the ultrasonic time is prolonged to 6 h. The results indicate that though the ultrasonic energy can cut the large-scaled GR into nanosheets (Fig. S3e), but the absence of template makes the cutting stress in all directions being equal, resulting into the generation of square nanosheets rather than nanoribbons.

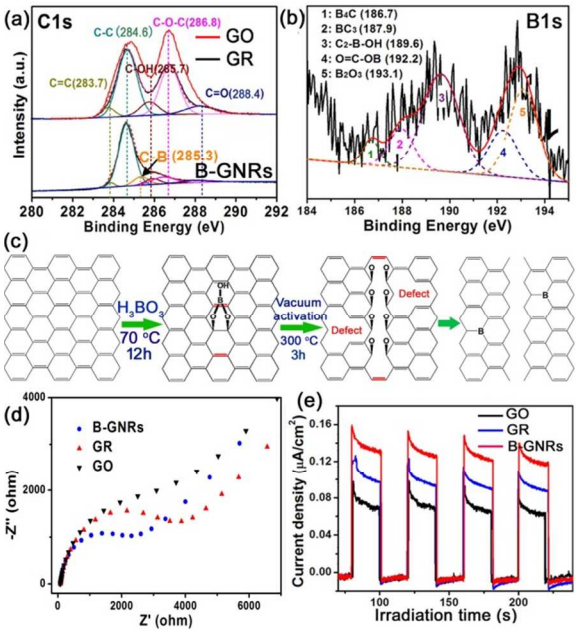

Fig. 2 C1s XPS spectra for GO, GR and B-GNRs (a). B1s XPS spectra for B-GNRs (b). The proposed chemical mechanism of nanosheets unzipping (c). EIS changes of GO, GR and B-GNRs electrodes (d). The EIS measurements were performed in the presence of a 2.5 mM $K_3[Fe(CN)_6]/K_4[Fe(CN)_6]$ (1:1) mixture as the electrochemical probe in a 0.1 M KCl aqueous solution; Transient photocurrent responses of GO, GR and B-GR in 0.5 M Na_2SO_4 aqueous solution under solar irradiation (e).

Fig. 2a is the C1s XPS spectra for the samples with and without H_3BO_3. Compared with the GR, after the addition of H_3BO_3, the characteristic peaks of C-OH and C-O-C at 285.7 and 286.8 eV on GNRs have an obviously decrease,[17] indicating that the doping of boron could improve the rupture of oxygen-containing groups, which is expected to the beneficial of the cutting of large-scaled GR into smaller sheets. Hence, the B-GNRs have a high conductivity compared with other carbon materials in herein. And a new peak of C-B generated at 285.3 eV in Fig. 2a, suggests the interaction between boron and graphene. Additionally, the B1s XPS spectra are also given to demonstrate the doping of boron in the skeleton of graphene and the formation of boron oxides on the surface of graphene

(Fig. 2b). The peaks of boron species are, from left to right, B_4C, BC_3, C_2-B-OH, O=C-OB and B_2O_3. The first two peaks account for the doping of boron in GNRs (B-GNRs),[10, 18] and the latter peaks of boron oxides indicate the interaction between graphene and surface covered boron oxides. Actually, the effect of the macro-residual stress induced by the boron oxides on the formation of nanoribbons, is very similar to the cutting of carbon nanotubes or graphene sheets into graphene nanoribbons or graphene quantum dots by the reoxidation and hydrothermal method (Fig. 2c).[2a, 19] Different from the hydrothermal method, the vacuum activation method can provide an anoxic environment, which is beneficial to the departing of oxygen atoms and the formation of lattice defects. These defects make the graphene sheets fragile and readily attacked by boron atoms.[20] Before the vacuum heating treatment, the H_3BO_3 is connected with graphene by the formation of B-O-C bonds, as shown in Fig. 2c. At the beginning of vacuum activation, the macro-residual stress of B-O-C bonds induces a rupture of C-C bond.[2a] The juxtaposition of the buttressing C-O bond combined with the departing force of oxygen in the vacuum condition, distorts the β, γ-alkenes (red in Fig. 2c), making them more prone to the next attack by boron oxides.[2a] These boron oxide groups tend to form a line on carbon lattice and the cooperative alignment induces a rupture of the underlying C-C bonds. With the increase of the heating temperature and heating time in the vacuum condition, the oxygen atoms on graphene are begin to depart from the skeleton to get the fully reduced GNRs. Meanwhile, some absorbed boron atoms replace the defect sites to achieve the doping of boron in GNRs. However, when the vacuum activation is replaced by a hydrothermal treatment, it is difficult to get GNRs even in the presence of H_3BO_3 (Fig. S4). That means an anoxic and negative pressure environment is very important to the playing of macro-residual stress for the generation of GNRs structures.

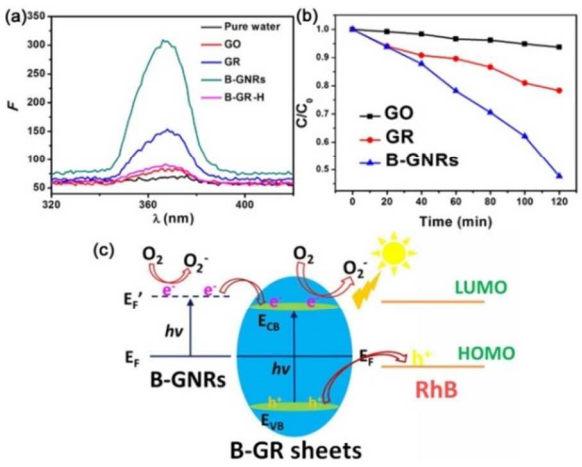

Fig. 3 Photoluminescence spectra of different samples (Measurement at room temperature under the excitation light at 280 nm, and B-GR-H means the boron doped graphene prepared by a hydrothermal method) (a). The photo-degradation of RhB (5 mg/L) under the UV light irradiation (b). The proposed photocatalysis mechanism of GR and B-GNRs under the UV light irradiation.

In our investigation, although the large-scaled graphene sheets have been cut into nanoribbons, it still has an excellent conductivity, which is much higher than GO and GR, as shown in Fig. 2d. The exposure of ZZ-edges makes the B-GNRs have semimetallic property with low impedance.[21] More interestingly, the B-GNRs can produce the electrons and exhibit a high photocurrent response under the simulated solar light irradiation, as shown in Fig. 2e. The boron doping and the exposure of AC edges make the B-GNRs become a semiconductor, which can produce photocurrent under the solar light irradiation. Tang et al.[10] have reported that the band gap of graphene could be controlled by adjusting the boron concentrations. In order to further prove the semiconductor property of B-GNRs, the photoluminescence (PL) spectra of different samples are shown in Fig. 3a. The GO has a low PL peak at 368 nm. After reduced in the vacuum, the fluorescence signal of GR has an obvious enhancing, and the B-GNRs emit the strongest PL, which is very similar to the PL spectra of some semiconductors, such as ZnO.[14] The low PL signal for the B-GR-H prepared by a hydrothermal method indicates the GNRs structure in our investigation is very important to the photo-generation of electrons (Fig. 3a). All the graphene based materials including GO, GR, B-GR, and B-GNRs can produce electrons under the irradiation of short wavelength light (λ=280 nm) owing to their semiconductor or semimetallic properties. The lowest impedance of B-GNRs indicates it should have a lowest PL intensity signal. However, B-GNRs has the strongest PL among all the graphene materials, which suggests a large number of electrons generated under the UV light irradiation, owing to its narrow bandgap and semimetallic property. The growth rate of electrons possibly overcomes the migration rate of electrons, which induces a strong PL signal for B-GNRs. Hence, we can conclude that the B-GNRs can produce electrons under the UV or solar light irradiation. With the doping of boron and the exposure of ZZ- and AC-edges, the B-GNRs possess tunable band gaps and p-type transport properties.[10] We believe the B-GNRs with controllable and predictable transport properties may pave a way for the development of graphene-based devices and the application to the graphene-based photocatalysis.

Fig. 3b shows the photocatalytic activities of graphene-based catalysts for the degradation of Rhodamine B (RhB, 5 mg/L) under the UV light irradiation. Compared with GO, the GR has an enhanced photocatalytic activity. Seen from the impedance results in Fig. 2d, the GO and GR all have semiconductor properties. In fact, the electronic property of graphene oxide is similar with that of graphite oxide, and both of them are semiconductors.[22] And the GR can also be considered as a reduced GO, due to its incomplete reduction in the vacuum at a relative low temperature. That is to say the GR is also a semiconductor. However, after boron doped in GR, its impedance has an obvious decrease, and the exposure of ZZ-edges in nanoribbons makes it has a semimetallic property. Our previous report has demonstrated that the HCl solution can wash out the impurities of boron oxides coated on the surface of catalyst.[23] Hence, the as-prepared samples have been washed by the HCl solution to eliminate the effect of boron oxides on the photocatalytic performance of B-GNRs. In our investigation, although there are some nanoribbons structures in B-GNRs, it also contains some boron doped GR sheets, as shown in Fig. 1c. B-GR has been demonstrated as a p-type semiconductor in photocatalysis.[2c, 10] Therefore, a heterojunction is formed when B-GR sheets contact with B-GNRs, as shown in Fig. 3c. The low conductivity of GO induces the low transfer efficiency of photo-produced electrons, which causes its lower photocatalytic activity. After activated in the vacuum, GR has an enhanced conductivity, correspondingly, its photoactivity is higher than GO's. Further doping with boron, the photo-produced electrons of B-GNRs make its Fermi level higher than the conduction band (E_{CB}) of B-GR sheets (from E_F to E'_F in Fig. 3c). The photo-produced electrons of B-GNRs are far more than the

electron densities on the E_{CB} of B-GR sheets (B-GNRs is a semimetal, while B-GR sheets is a semiconductor). Therefore, there is an enough driving force to transfer the electrons from B-GNRs to B-GR (Fig. 3c). The transferred electrons on the E_{CB} of B-GR sheets are consumed by O_2 to form the reactive species of $O_2^{-\bullet}$. On the other hand, the photo-generated holes of B-GR sheets can inject into the HOMO of RB as a result of the p-type semiconductor property and the more positive potential of the valence band (E_{VB}) in B-GR. Hence, compared with the blank GR and GO sheets, the photo-generated electrons and holes of B-GNRs are more effectively separated under the UV light irradiation. Moreover, the high carrier mobility of B-GNRs is in favor of fast electron transport, which inhibits the recombination of photo-generated electron-hole pairs and enhances the photocatalytic performance of B-GNRs.

In conclusion, Boron doped GNRs is successfully synthesized by a simple vacuum activation method. The B-GNRs exhibits an excellent electronic conductivity and high photocatalytic activity for the degradation of RhB. The doping of boron induces the formation of GNRs structures and the exposure of ZZ- and AC-edges, which make it having a semimetallic property. That is, B-GNRs not only have the excellent conductivities, but also have the controllable bandgaps and predictable electrons transport properties, which determine its large potential application to the graphene-based photoelectric devices and photocatalysis.

This work has been supported by National Nature Science Foundation of China (21173077, 21377038, 21237003 and 21203062), National Basic Research Program of China (973 Program, 2013CB632403), the Project of International Cooperation of the Ministry of Science and Technology of China (No. 2011DFA50530); Science and Technology Commission of Shanghai Municipality (12230705000, 12XD1402200), the Research Fund for the Doctoral Program of Higher Education (20120074130001) and the Fundamental Research Funds for the Central Universities.

Notes and references

Key Laboratory for Advanced Materials and Institute of Fine Chemicals, East China University of Science and Technology, Shanghai (China)

† Corresponding Author: E-mail: jlzhang@ecust.edu.cn, Fax: +86-21-64252062.

Electronic Supplementary Information (ESI) available: [details of any supplementary information available should be included here]. See DOI: 10.1039/c000000x/

1 (a) K. S. Novoselov, A. K. Geim, S. V. Morozov, D. Jiang, Y. Zhang, S. V. Dubonos, I. V. Grigorieva and A. A. Firsov, *Science*, 2004, **306**, 666; (b) C. N. R. Rao, A. K. Sood, K. S. Subrahmanyam and A. Govindaraj, *Angew. Chem. Int. Ed.*, 2009, **48**, 7752; (c) H. Hu, Z. Zhao, W. Wan, Y. Gogotsi and J. Qiu, *Adv. Mater.*, 2013, **25**, 2219; (d) X. Huang, K. Qian, J. Yang, J. Zhang, L. Li, C. Yu and D. Zhao, *Adv. Mater.*, 2012, **24**, 4419; (e) S. Ding, J. S. Chen, D. Luan, F. Y. C. Boey, S. Madhavi and X. W. Lou, *Chem. Commun.*, 2011, **47**, 5780.

2 (a) D. V. Kosynkin, A. L. Higginbotham, A. Sinitskii, J. R. Lomeda, A. Dimiev, B. K. Price and J. M. Tour, *Nature*, 2009, **458**, 872; (b) X. Li, X. Wang, L. Zhang, S. Lee and H. Dai, *Science*, 2008, **319**, 1229; (c) R. Lv and M. Terrones, *Mater. Lett.*, 2012, **78**, 209.

3 M. Y. Han, B. Özyilmaz, Y. Zhang and P. Kim, *Phys. Rev. Lett.*, 2007, **98**, 206805.

4 Y.-W. Son, M. L. Cohen and S. G. Louie, *Phys. Rev. Lett.*, 2006, **97**, 216803.

5 M. Ezawa, *Phys. Rev. B*, 2006, **73**, 045432.

6 D. A. Areshkin, D. Gunlycke and C. T. White, *Nano Lett.*, 2006, **7**, 204.

7 F. Schwierz, *Nat. Nanotechnol.*, 2010, **5**, 487.

8 A. León, Z. Barticevic and M. Pacheco, *Microelectronics J.*, 2008, **39**, 1239.

9 X. Wang, X. Li, L. Zhang, Y. Yoon, P. K. Weber, H. Wang, J. Guo and H. Dai, *Science*, 2009, **324**, 768.

10 Y.-B. Tang, L.-C. Yin, Y. Yang, X.-H. Bo, Y.-L. Cao, H.-E. Wang, W.-J. Zhang, I. Bello, S.-T. Lee, H.-M. Cheng and C.-S. Lee, *ACS Nano*, 2012, **6**, 1970.

11 F. Cervantes-Sodi, G. Csányi, S. Piscanec and A. C. Ferrari, *Phys. Rev. B*, 2008, **77**, 165427.

12 (a) D. Wei, Y. Liu, H. Zhang, L. Huang, B. Wu, J. Chen and G. Yu, *J. Am. Chem. Soc*, 2009, **131**, 11147; (b) C. Di, D. Wei, G. Yu, Y. Liu, Y. Guo and D. Zhu, *Adv. Mater.*, 2008, **20**, 3289; (c) K. S. Kim, Y. Zhao, H. Jang, S. Y. Lee, J. M. Kim, K. S. Kim, J.-H. Ahn, P. Kim, J.-Y. Choi and B. H. Hong, *Nature*, 2009, **457**, 706.

13 (a) M. Xing, J. Zhang, F. Chen and B. Tian, *Chem. Commun.*, 2011, **47**, 4947; (b) T. Xia, W. Zhang, J. B. Murowchick, G. Liu and X. Chen, *Adv. Energy Mater.*, 2013, **3**, 1516.

14 D. I. Son, B. W. Kwon, D. H. Park, W.-S. Seo, Y. Yi, B. Angadi, C.-L. Lee and W. K. Choi, *Nat. Nanotechnol.*, 2012, **7**, 465.

15 M. Terrones, A. R. Botello-Méndez, J. Campos-Delgado, F. López-Urías, Y. I. Vega-Cantú, F. J. Rodríguez-Macías, A. L. Elías, E. Muñoz-Sandoval, A. G. Cano-Márquez, J.-C. Charlier and H. Terrones, *Nano Today*, 2010, **5**, 351.

16 H. Raza and E. C. Kan, *Phys. Rev. B*, 2008, **77**, 245434.

17 (a) H.-K. Jeong, Y. P. Lee, R. J. W. E. Lahaye, M.-H. Park, K. H. An, I. J. Kim, C.-W. Yang, C. Y. Park, R. S. Ruoff and Y. H. Lee, *J. Am. Chem. Soc.*, 2008, **130**, 1362; (b) W. Chen, L. Yan and P. R. Bangal, *J. Phys. Chem. C*, 2010, **114**, 19885.

18 (a) H.-L. Guo, X.-F. Wang, Q.-Y. Qian, F.-B. Wang and X.-H. Xia, *ACS Nano*, 2009, **3**, 2653; (b) Z.-H. Sheng, L. Shao, J.-J. Chen, W.-J. Bao, F.-B. Wang and X.-H. Xia, *ACS Nano*, 2011, **5**, 4350; (c) Z.-H. Sheng, H.-L. Gao, W.-J. Bao, F.-B. Wang and X.-H. Xia, *J. Mater. Chem.*, 2012, **22**, 390.

19 (a) D. Pan, J. Zhang, Z. Li and M. Wu, *Adv. Mater.*, 2010, **22**, 734; (b) C. H. A. Wong, C. K. Chua, B. Khezri, R. D. Webster and M. Pumera, *Angew. Chem. Int. Ed.*, 2013, **52**, 8685.

20 L. Zhao, M. Levendorf, S. Goncher, T. Schiros, L. Pálová, A. Zabet-Khosousi, K. T. Rim, C. Gutiérrez, D. Nordlund, C. Jaye, M. Hybertsen, D. Reichman, G. W. Flynn, J. Park and A. N. Pasupathy, *Nano Lett.*, 2013, **13**, 4659.

21 (a) Z. Li, J. Yang and J. G. Hou, *J. Am. Chem. Soc.*, 2008, **130**, 4224; (b) B. Biel, F. Triozon, X. Blase and S. Roche, *Nano Lett.*, 2009, **9**, 2725.

22 (a) C. Chen, W. Cai, M. Long, B. Zhou, Y. Wu, D. Wu and Y. Feng, *ACS Nano*, 2010, **4**, 6425; (b) Z. Luo, P. M. Vora, E. J. Mele, A. T. C. Johnson and J. M. Kikkawa, *Appl. Phys. Lett.*, 2009, **94**.

23 M. Xing, W. Fang, M. Nasir, Y. Ma, J. Zhang and M. Anpo, *J. Catal.*, 2013, **297**, 236.

